Published in final edited form as:
Macromolecules. 2010 November 9; 43(21): 9181–9190. doi:10.1021/ma101860t.

Chains are more flexible under tension

Andrey V. Dobrynin[1], **Jan-Michael Y. Carrillo**[1], and **Michael Rubinstein**[2]

[1]Polymer Program, Institute of Materials Science and Department of Physics, University of Connecticut, Storrs, CT 06269

[2]Department of Chemistry, University of North Carolina, Chapel Hill, NC 27599-3290

Abstract

The mechanical response of networks, gels, and brush layers is a manifestation of the elastic properties of the individual macromolecules. Furthermore, the elastic response of macromolecules to an applied force is the foundation of the single-molecule force spectroscopy techniques. The two main classes of models describing chain elasticity include the worm-like and freely-jointed chain models. The selection between these two classes of models is based on the assumptions about chain flexibility. In many experimental situations the choice is not clear and a model describing the crossover between these two limiting classes is therefore in high demand. We are proposing a unified chain deformation model which describes the force-deformation curve in terms of the chain bending constant K and bond length b. This model demonstrates that the worm-like and freely-jointed chain models correspond to two different regimes of polymer deformation and the crossover between these two regimes depends on the chain bending rigidity and the magnitude of the applied force. Polymer chains with bending constant $K>1$ behave as a worm-like chain under tension in the interval of the applied forces $f \leq Kk_BT/b$ and as a freely-jointed chain for $f \geq Kk_BT/b$ (k_B is the Boltzmann constant and T is the absolute temperature). The proposed crossover expression for chain deformation is in excellent agreement with the results of the molecular dynamics simulations of chain deformation and single-molecule deformation experiments of biological and synthetic macromolecules.

A polymer **c**hain under tension is one of the classical problems of polymer physics.[1] The solution of this problem is of paramount importance for understanding swelling and deformation of polymeric and biological networks and gels, [1–3] deformation of polymer chains in external flow,[4] for elucidating factors controlling structure of polymer brushes,[5, 6] and for analysis of force-spectroscopy experiments.[7–9] The force spectroscopy experiments on DNA, RNA, actin, and microtubules filaments provide information about stresses and strains experienced by molecules during biological processes such as molecular recognition between DNA and proteins, protein-induced bending of DNA, cytoskeleton polymerization, and energy transduction during the ATP cycle in molecular motors.[7–9] Unfortunately, the interpretation of the force-elongation experiments and the obtained values of elastic constants is model-dependent and heavily relies on the assumptions used in the data analysis.

There are several models developed to describe chain deformation.[1] The freely-jointed class of chain models[1] is usually applied to the deformations of flexible polymers. The deformations of stiff biological macromolecules such as DNA and biological filaments are described by the class of worm-like chains.[9–11] In the small force limit, the models from both classes give a linear relationship between the magnitude of the applied force f and the

Correspondence to: Andrey V. Dobrynin.

chain elongation along the force direction R_f. [1] But at large pulling forces, the models from these two classes demonstrate qualitatively different power law dependences of the tension f on the difference between the chain size R_f and its maximum value R_{max}. For the models belonging to the class of freely-jointed chains, the force is inversely proportional to this difference, $f \propto (R_{\max} - R_f)^{-1}$, while for the models from the class of the worm-like chains, the force f exhibits a stronger divergence $f \propto (R_{\max} - R_f)^{-2}$.

Computer simulations of chain models with finite bending rigidity show the existence of two nonlinear deformation regimes under tension.[12, 13,14] In the interval of the applied forces f smaller than the crossover value f_c, a polymer chain behaves as a worm-like chain with force proportional to $f \propto (R_{\max} - R_f)^{-2}$. However, when the value of the applied force f exceeds the critical value f_c, one observes the freely-jointed chain behavior $f \propto (R_{\max} - R_f)^{-1}$. The crossover between these two nonlinear deformation regimes is model dependent and is controlled by the chain bending rigidity. The theoretical interpretation of these results was done on the scaling level by introducing force-dependent chain persistence length[14] or by using asymptotic results for strong chain deformations.[12, 13] These approximations are reasonably good for very stiff chains for which the crossover between different nonlinear deformation regimes occurs in the limit of large chain deformations. However, for less stiff and more flexible chains the crossover is located in the intermediate range of chain deformations and the proposed approximations lead to large errors. Furthermore, the majority of experimental systems, for which crossover between different deformation regimes can be observed, belong to the class of flexible polymers. Thus, accurate interpretation of the experimental results requires a more precise expression describing chain deformation in the entire interval of the applied forces.

In this paper we study a discrete chain model with a bending potential. This model has a parameter – the effective bending constant – by changing which one can crossover between worm-like (WLC) and freely-jointed chain (FJC) models. We present analytical solutions of this model that provide a crossover expression describing chain deformations in the entire interval of the applied forces with an accuracy better than 1%. We used this expression to describe the crossover between worm-like and freely-jointed chain models in terms of the chain rigidity and the magnitude of the applied force. Application of our expression to the results of single molecule experiments and computer simulations suggests universality of the force-elongation dependence of polymer chains.

Consider a chain with N bonds of constant length b. The ends of this chain are pulled by a pair of external forces of equal magnitude f and opposite directions. For simplicity we will assume that these external forces are parallel to the z-axis. We can describe a chain conformation by a set of unit vectors $\vec{n}_i$ pointing along the chain bonds. The potential energy of the chain with the bending modulus k_BTK (where k_B is the Boltzmann constant, T *is* the absolute temperature and K is the chain bending constant) in a given conformation includes contributions from the bending energy and from the external forces

$$\frac{U\left(\{\vec{n}_i\},\vec{f}\right)}{k_BT} = \frac{K}{2}\sum_{i=0}^{N-2}(\vec{n}_i - \vec{n}_{i+1})^2 - \sum_{i=0}^{N-1}\frac{b\left(\vec{f}\cdot\vec{n}_i\right)}{k_BT} \quad (1)$$

The first term in the right hand side of eq 1 describes the chain bending rigidity. The value of the parameter K controls the orientational correlations between bond vectors. In the case of the large values of the parameter $K \gg 1$, the potential energy of a polymer in our model (eq 1) describes a worm-like chain under tension. However, as the value of the parameter K approaches zero, $K \to 0$, our model (eq 1) describes the deformation of a freely-jointed

chain. Thus, by varying the value of the bending constant K one can cover both worm-like and freely-jointed chain regimes.

We can evaluate chain deformation in the two limiting cases of small and large values of the applied forces. In the limit of weak forces we can consider the force term in the r.h.s. of eq 1 as a perturbation. Using this approximation, the average value of the projection of the unit bond vector on the force direction is equal to

$$\langle n_z\rangle = \left\langle N^{-1}\sum_{s=0}^{N-1} n_s^z \right\rangle \approx \frac{fb}{3k_BTN}\sum_{s,j=0}^{N-1}\left\langle\left(\vec{n}_s\cdot\vec{n}_j\right)\right\rangle_0 \approx \frac{fb_K}{3k_BT}, \quad \text{for } fb_K<<k_BT \tag{2}$$

where brackets $\langle\ \rangle$ and $\langle\ \rangle_0$ denote averages with the statistical weights corresponding to the chain's potential energy $U(\{\vec{n}_i\}, f)$ with and without force respectively (see eq 1). This chain deformation regime is referred to as *the linear deformation regime* in the chain deformation diagram shown in reduced force $\tilde{f} = fb/k_BT$ - bending constant K plane (see Figure 1). The Kuhn length in our model is equal to

$$b_K = b\frac{1+\langle\cos(\theta)\rangle_0}{1-\langle\cos(\theta)\rangle_0} = b\frac{1+\coth(K)-K^{-1}}{1-\coth(K)+K^{-1}} \approx \begin{cases} 2bK, & \text{for } K>>1 \\ b, & \text{for } K<<1 \end{cases} \tag{3}$$

It depends on the average value $\langle\cos(\theta)\rangle_0$ of the cosine of the angle θ between two consecutive bond vectors along the polymer backbone. Note, that in the case of large values of the bending parameter $K\gg1$, the Kuhn length is equal to $b_K = 2bK$. In the opposite limit $K\ll1$ the Kuhn length approaches the bond length b. The average projection of the end-to-end vector on the direction of deformation is related to the average value of the projection of the unit bond vector on the direction of the applied force $\langle n_z\rangle$ by the equation

$$\langle R_z\rangle = Nb\langle n_z\rangle \tag{4}$$

In the case of large magnitude of the applied force, $f > k_BT/b_K$, the average value of the projection of the unit vector on the direction of the applied force $\langle n_z\rangle$ is close to unity. In this regime we can perform the mode spectrum analysis of the bond vectors $\vec{n}_i$ (see Appendix A). This approach shows that the chain deformation and the magnitude of the applied force are related as follows

$$1-\langle n_z\rangle^2 \approx 2\langle n_z\rangle\left(\tilde{f}\left(4K\langle n_z\rangle+\tilde{f}\right)\right)^{-1/2}, \quad \text{for } b/b_K<\tilde{f} \tag{5}$$

Eq 5 can be transformed to the quadratic equation for the reduced force. The solution of this equation gives the relationship between the normalized external force $\tilde{f}$ and chain size $\langle R_z\rangle$ (or average projection of the bond unit vector $\langle n_z\rangle$ see eq 4) in the nonlinear deformation regime.

$$\tilde{f} \approx 2\langle n_z\rangle K\left(\sqrt{1+\frac{1}{K^2\left(1-\langle n_z\rangle^2\right)^2}}-1\right), \quad \text{for} \quad b/b_K<\tilde{f} \tag{6}$$

The interesting consequence of this equation is that there are two nonlinear regimes of the pulling force dependence on the average chain extension. In the intermediate force interval $b/b_K < \tilde{f} \ll K$ (or $K^{-1} \ll 1 - \langle n_z \rangle^2 \ll 1$, eq 6 reduces to

$$\tilde{f}K \approx \frac{\langle n_z \rangle}{\left(1 - \langle n_z \rangle^2\right)^2} \approx \frac{1}{4(1 - \langle n_z \rangle)^2}, \quad \text{for } b/b_K < \tilde{f} << K \tag{7.a}$$

This is exactly the expected dependence for the worm-like class of polymer chains under tension.[1] Note that the width of this regime shrinks with decreasing bending constant K (see *nonlinear WLC deformation regime* in Figure 1).

In the opposite limit of very large forces $\tilde{f} \gg K$ (or $1 - \langle n_z \rangle^2 \ll K^{-1} \ll 1$) we obtain

$$\tilde{f} \approx \frac{2\langle n_z \rangle}{1 - \langle n_z \rangle^2} \approx \frac{1}{1 - \langle n_z \rangle}, \quad \text{for } \tilde{f} >> K \tag{7.b}$$

Thus, our model in the large force limit behaves as a freely-jointed chain with polymer deformation being independent on the bending rigidity K (see *nonlinear FJC deformation regime* in Figure 1). This should not be surprising since in this limit the force term in eq 1 dominates over the bending term, and controls chain elasticity at length scales smaller than the Kuhn length.

A more accurate location of the crossover between the nonlinear WLC and nonlinear FJC deformation regimes can be obtained by equating eqs 7a and 7b, solving the resultant equation for $\langle n_z \rangle \approx (1 - 1/(2K))^{1/2}$ and substituting this solution into eq 6. This results in the following equation describing the crossover line

$$\tilde{f}_c \approx 2.47K(1 - 0.5/K)^{1/2} \tag{8}$$

This equation is shown as a solid line separating *nonlinear FJC deformation regime* and *nonlinear WLC deformation regime* in Figure 1. Note, that eq 6 describing the nonlinear chain deformation can be reduced to the expressions derived in ref.[12] by setting $\langle n_z \rangle \approx 1$ and approximating $1 - \langle n_z \rangle^2$ by $2(1 - \langle n_z \rangle)$.

Combining the force-elongation relation (eq 6) for the nonlinear chain deformations ($1 - \langle n_z \rangle^2 \ll 1$) with eq 2 for the linear chain deformation regime ($\langle n_z \rangle^2 \ll 1$) we propose a crossover expression which describes polymer deformation in the entire interval of applied forces

$$\frac{f}{k_B T} \approx \frac{3\langle n_z \rangle}{b_K} + \frac{2\langle n_z \rangle}{b}\left(\sqrt{K^2 + \left(1 - \langle n_z \rangle^2\right)^{-2}} - \sqrt{K^2 + 1}\right) \tag{9}$$

where we have added terms $\langle n_z \rangle \left(3/b_K + 2\left(K - \sqrt{K^2+1}\right)/b\right)$ linear in $\langle n_z \rangle$ to assure the proper linear force-extension dependence (see eq 2). Eq 9 is the main result of this paper. Note, that for the discrete chain model with bending potential (eq 1) the Kuhn length depends on the bond length b and the value of the bending constant K (see eq 3). Thus, there are only two independent parameters that describe chain deformation. The Kuhn length b_K determines chain elastic response at small deformations and the crossover to the nonlinear regime ($f \approx$

k_BT/b_K), while the bending constant K controls force-elongation dependence in the intermediate range of the applied forces and the crossover ($f \approx \tilde{f}_c k_BT/b$) between nonlinear worm-like chain deformation regime and nonlinear freely-jointed chain deformation regime (see Figure 1). It is interesting to point out that in the limit of large K for which $b_K \approx 2Kb$ eq 9 reduces to the expression for the deformation of semiflexible chains derived in ref 15.

$$\frac{fbK}{k_BT} \approx \frac{\langle n_z \rangle}{2} + \frac{\langle n_z \rangle}{\left(1 - \langle n_z \rangle^2\right)^2}, \quad \text{for } \tilde{f} < \tilde{f}_c \tag{10}$$

Below we test our model of chain deformation by analysing the single molecule force-extension data from computer simulations and experiments (the details of this analysis are given in Appendices B and C respectively).

In order to test how well eq 9 describes chain deformation we have performed simulations of the bead-spring chains consisting of $N_m=200$ monomers with different values of the bending constant K. The simulation details are provided in Appendix B. Figure 2 displays the results of the molecular dynamics simulations of these chains under tension. The lines correspond to eq 9 where the Kuhn lengths b_K were calculated from the value of the bending constant K using the theoretical expression for this model (see eq 3) and the bond length b was obtained from simulations for each set of bond potential parameters (see Appendix B). The agreement between the analytical expression for the chain deformation (eq 9) and the simulation results is excellent. The deviation between the simulations and the theoretical curves is less than 1% throughout the entire interval of chain deformations. There is a slightly larger deviation (~3%) of the analytical expression from the simulation results for chains with $K>25$ in the small force limit. For these chains the Kuhn length $b_K \approx 2bK$ approaches their contour length bN and one has to keep all terms in the sum in the eq 2 to correctly account for the finite N effects.

We have also used simulation results to compare the accuracy of different chain deformation models (see Appendix D). [12, 14] The analysis shows that our eq 9 is the most accurate expression describing chain deformation in the entire interval of the applied forces. For example, for chain with K=1 the maximum deviation of eq 9 from the simulation results does not exceed 1%. At the same time, the expression by Rosa et al.[12] shows a deviation of 6% for $\langle n_z \rangle \approx 0.5$. Even larger error ~ 10–15% in the same chain deformation range is observed for the Toan and Thirumalai expression.[14] The difference between expressions drops to less than 1% when the chain deformation $\langle n_z \rangle$ exceeds 0.9. The detailed comparison between different chain deformation models can be found in Appendix D.

For the other models, such as freely-rotating chain model, [1] the effective bending potential can only be defined for a sequence of several bonds. We need to define effective bonds of length b_e and effective bending constant K_e to map the force-elongation curves for this chain model onto our model (eq. 1). For the discrete chain model the value of the effective bond length b_e and the value of the effective bending constant K_e are related to each other by the equation analogous to eq 3

$$b_e = b_K \frac{1 - \coth(K_e) + K_e^{-1}}{1 + \coth(K_e) - K_e^{-1}} \tag{11}$$

The Kuhn length b_K for the freely-rotating chain model can be calculated from the analytical expression (see eq B.5).[1] In this case we can substitute eq 11 for the effective bond length b_e

into eq 9 and use eq 9 to evaluate the value of the bending constant K_e by fitting the chain deformation data to eq 9.

Figure 3 shows results of the molecular dynamics simulations of the freely-rotating chain model (see Appendix B for details). The lines correspond to the best fit to eq 9 by considering K_e as adjustable parameter. Inset shows the dependence of the effective chain bending constant on the value of the bond angle. Once again we see an excellent agreement between simulation and analytical results (see Appendix B for details).

Similar analysis can be applied to describe deformation of other chain models[1] as well as experiments. To illustrate this we have performed simulations of deformation of a chain with hindered internal rotations[1] and with the force field parameters corresponding to polyethylene chain.[16] For this chain model the force elongation curve is close to that of a freely-rotating chain with the value of the bond angle 50° (see Figure 3).

We applied eq 9 together with eq 11 to reanalyse the experimental data on single chain deformation. In Figure 4 we plotted dependence of the effective chain bending constant K_e on the ratio b_K/b_e of the Kuhn length to the effective bond length b_e for several different polymers including the single stranded DNA at different salt concentrations,[17] polymethacrylic acid,[18] polystyrene,[19] polydimethylsiloxane,[20] dextran,[21] methlycellulose, [22] double stranded DNA,[23] N2B domain of titin, and PEVK domain of titin[24] (see Appendix C for details). The data follow the line obtained for parameters of the discrete chain model with bending potential (eq 11) indicating a successful mapping of the real polymeric systems on our model.

In order to illustrate universality of the crossover between FJC and WLC for chains described by different chain models and for experiments we combined simulation data for the discrete chain model with bending potential (eq 1), the freely-rotating chain model, chain with hindered internal rotations and experimental data and show in Figure 5 the dependence of the reduced force $\frac{\tilde{f}_e}{\langle n_z\rangle K_e}$ on the parameter $K_e(1-\langle n_z\rangle^2)$. The dashed line on this plot corresponds to the eq 5 that describes both nonlinear deformation regimes as well as the crossover between them very well

$$\frac{\tilde{f}_e}{\langle n_z\rangle K_e} \approx 2\left(\sqrt{1+\frac{1}{K_e^2\left(1-\langle n_z\rangle^2\right)^2}}-1\right), \qquad \text{for } b_e/b_K<\tilde{f}_e \tag{12}$$

Note that for the discrete chain model with bending potential (see eq 1) $K_e=K$ and $b_e=b$. One can clearly identify two nonlinear chain deformation regimes in Figure 5. In the intermediate force interval $k_BT/b_K < f < K_e k_BT/b_e$, we observe the power law scaling $f \propto (1-\langle n_z\rangle^2)^{-2}$ representative of the worm-like chain behaviour, while in the large force limit, $K_e k_BT/b_e < f$, the scaling dependence changes to $f \propto (1-\langle n_z\rangle^2)^{-1}$. The surprising result of this plot is that even chains with bending constants K=1 and 2 which one would consider to be flexible chains still exhibit a worm-like chain deformation dependence of the chain elongation on the applied force in the intermediate force range. The deviation from the universal curve at weak forces represents the crossover to the linear deformation regime with the average value of the projection of the unit bond vector on the direction of the applied force $\langle n_z\rangle$ proportional to the force f (see Appendix A for details). Note that the deviation from the universal behaviour should also be observed in the limit of very large forces when chain elongation results in the deformation of the bond angles and bond lengths. [9,11]

The force f_c corresponding to the crossover between the worm-like and freely-jointed chain regimes depends on the value of the effective bending rigidity K_e and effective bond length b_e. Using eq 8 we can estimate the typical interval of forces where the crossover to the nonlinear FJC deformation regime can be observed for different experimental systems. For example, for flexible chains such as single stranded DNA with a Kuhn length on the order of 1 – 1.5 *nm* this crossover occurs between 10 and 100 *pN* showing an increase with decreasing salt concentration (see Table C1). In the case of a rigid molecule such as double stranded DNA with the persistence length on the order of 40 *nm* the upper boundary of the worm-like chain regime is located at $f \propto 4nN$ which is outside the range of stability of double helix. Therefore one can safely use the worm-like chain model in the entire interval of the accessible forces for double stranded DNA.

For simplicity, we did not take into account the interactions between the monomers that are remote along the polymer backbone. These interactions lead to chain swelling and can alter the chain behaviour in the weak force limit.[1] However, we don't expect these effects to be significant in the case of nonlinear chain deformation and to change the crossover between wormlike and freely-jointed chain deformation regimes. The excluded volume interactions can only influence the location of the crossover to linear chain deformation regime. Note that our model can also be extended to include effect of the bond elongation using the formalism developed in ref 15.

In conclusion, we have derived the crossover expression for chain deformation (eq 9) which correctly describes chain elongation in the entire interval of the applied forces. This expression confirms the existence of two nonlinear chain deformation regimes. With increasing force magnitude the chain deformation first scales with the applied force as $\langle R_z \rangle / R_{max} \propto 1 - (fK_e b_e / k_B T)^{-1/2}$ and then as $\langle R_z \rangle / R_{max} \propto 1\text{-}(fb_e / k_B T)^{-1}$. The force corresponding to the crossover between these two regimes is a function of the chain flexibility and is controlled by the effective bending rigidity K_e and the effective bond length b_e. Our expression (eq 9) is in excellent agreement with the simulations results to an accuracy better than 1%. This expression for the force-deformation curve was used for the interpretation of the force spectroscopy data by considering b_K and K_e as fitting parameters. This allowed us to express parameters of the real polymeric systems in terms of the parameters describing deformation of the discrete chain model with bending potential (see eq 1).

The model of chain deformation presented in this paper can be applied to describe nonlinear elasticity of biological and polymeric networks and gels,[1–3, 25] chain deformation in brush layers,[5] and structure of polyelectrolyte chains in dilute and semidilute polyelectrolyte solutions where electrostatic forces between ionized groups can result in strong chain elongation.[26] Our approach can also be extended to model deformation of molecular brushes and branched macromolecules.[27]

Acknowledgments

The authors are grateful to Prof. O. Saleh for providing the original data on ssDNA deformation. This work was supported by the National Science Foundation under the grant DMR-1004576, CHE-0911588, DMR-0907515, and CBET-0609087, and by the National Institutes of Health under grant 1-R01-HL077546-03A2.

Appendix A. Mode Spectrum Analysis of Chain Deformation

Below we present details of the mode spectrum analysis of the chain's potential energy given by eq 1 extending the formalism developed in ref 15. In order to calculate averages with the Boltzmann weights corresponding to the chain's potential energy given by eq 1, it is useful to introduce the normal coordinates for a set of the bond vectors $\{\vec{n}_i\}$

$$\vec{n}_s = \sum_{k=-(N-1)}^{N-1} \vec{a}_k \exp\left(i\frac{\pi k s}{N}\right) \tag{A.1}$$

In this representation the chain's potential energy is the quadratic function of the mode amplitudes

$$\frac{U(\{\vec{a}_k\}, f, \mu)}{k_B T} = N \sum_{k=-(N-1)}^{N-1} \left(G(k)\frac{(\vec{a}_k \cdot \vec{a}_{-k})}{2} - \tilde{f} a_k^z t_k\right) \tag{A.2}$$

where we defined functions

$$G(k) = 2K(1 - \cos(k\pi/N)) \tag{A.3}$$

$$t_k = \frac{1}{N}\sum_{s=0}^{N-1} \exp\left(i\frac{\pi k s}{N}\right), \tag{A.4}$$

and used the expression for the reduced force $\tilde{f} = fb/k_BT$.

In the normal mode representation, the bond-bond correlation function $G(l)$ describing the decay of the orientational memory along the polymer backbone

$$G(l) = \frac{1}{N-l}\sum_{s=0}^{N-l-1} \left\langle\left(\vec{n}_s \cdot \vec{n}_{s+l}\right)\right\rangle \tag{A.5}$$

is equal to

$$G(l) = \sum_{k=-(N-1)}^{N-1} \left\langle\left(\vec{a}_k \cdot \vec{a}_{-k}\right)\right\rangle \exp\left(i\frac{k\pi l}{N}\right). \tag{A.6}$$

It is important to point out that the normal modes are not independent. This is due to the constraint on the value of the bond-bond correlation function $G(l)$ at l=0, which should be equal to unity

$$1 = \sum_{k=-(N-1)}^{N-1} \left\langle\left(\vec{a}_k \cdot \vec{a}_{-k}\right)\right\rangle. \tag{A.7}$$

In order to account for this constraint, we will introduce a Lagrange multiplier μ, and modify the expression for the chain's potential energy as follows

$$\frac{U\left(\left\{\vec{a}_k\right\},f,\mu\right)}{k_BT}=N\sum_{k=-(N-1)}^{N-1}\left[(G(k)+\mu)\frac{(\vec{a}_k\cdot\vec{a}_{-k})}{2}-\tilde{f}t_ka_k^z\right]-\frac{N\mu}{2}. \tag{A.8}$$

The complication in calculating averages with the chain's potential energy, given by eq A.8, arises because it requires knowledge of the orientations of the vector $\vec{a}_k$. Let us evaluate averages over mode amplitudes in two limiting cases of small and large values of the applied force. In the small force limit, $\tilde{f}\ll 1$, we can consider the force term in the r.h.s. of the eq A. 2 as a perturbation. In this approximation the average value of the projection of the unit bond vector on the direction of the force is equal to

$$\langle n_z\rangle=\left\langle N^{-1}\sum_{s=0}^{N-1}n_s^z\right\rangle=\sum_{k=-(N-1)}^{N-1}\left\langle a_k^z\right\rangle t_k\approx N\tilde{f}\sum_{k=-(N-1)}^{N-1}\left\langle\left(a_k^za_{-k}^z\right)\right\rangle_0t_kt_{-k}, \tag{A.9}$$

where brackets $\langle\ \rangle$ and $\langle\ \rangle_0$ denote averages with the statistical weights corresponding to $U(\left\{\vec{a}_k\right\},f,\mu)$ and $U(\left\{\vec{a}_k\right\},0,\mu)$ respectively. In order to calculate the averages in eq A.9 we will set $\vec{a}_k=\vec{a}_{-k}$ and consider interval $k\geq 0$. This results in the following relations

$$\begin{aligned}\left\langle\left(a_0^z\right)^2\right\rangle_0&=\frac{\left\langle\vec{a}_0^{\,2}\right\rangle_0}{3}=\frac{2}{3\mu N}\\ \left\langle\left(a_k^z\right)^2\right\rangle_0&=\frac{\left\langle\vec{a}_0^{\,2}\right\rangle_0}{3}=\frac{(G(k)+\mu)^{-1}}{3N}.\end{aligned} \tag{A.10}$$

Note that in this approximation each vector $\vec{a}_k$ has only two independent components because eq A.1 is a linear transformation. Taking eqs A.10 into account, the r.h.s of eq A.9 reduces to

$$\langle n_z\rangle\approx\frac{2\tilde{f}}{3\pi N}\sum_{s,s'=0}^{N-1}\int_0^\pi\frac{dq\cos(q(s-s'))}{G(q)+\mu}=\frac{\tilde{f}\left\langle R_0^2(\mu,K)\right\rangle}{3N},\ \text{for } \tilde{f}<<1 \tag{A.11}$$

where we defined

$$\left\langle R_0^2(\mu,K)\right\rangle=\frac{2}{\pi}\sum_{s,s'=0}^{N-1}\int_0^\pi\frac{dq\cos(q(s-s'))}{G(q)+\mu}. \tag{A.12}$$

In obtaining eq A.11 we have introduced $q=k\pi/N$, and substituted summation by integration.

In the case of large force amplitudes, we can assume that the average component of the vectors $\vec{a}_k$ points in the direction of the applied force. Thus, the addition of the external constant force changes the average value of the amplitude of the mode component along z-axis to

$$\left\langle a_k^z\right\rangle\approx\tilde{f}t_{-k}/(G(k)+\mu),\quad\text{for } \tilde{f}>>1 \tag{A.13}$$

resulting in the following expression for the average value of the unit bond vector

$$\langle n_z\rangle \approx \sum_{k=-(N-1)}^{N-1}\left\langle a_k^z\right\rangle t_k \approx \frac{2\tilde{f}}{N\pi}\sum_{s,s"=0}^{N-1}\int_0^\pi \frac{dq\cos((s-s')q)}{G(q)+\mu} - \frac{\tilde{f}}{\mu} = \frac{\tilde{f}\left\langle R_0^2(\mu,K)\right\rangle}{N} - \frac{\tilde{f}}{\mu}. \tag{A.14}$$

Combining eqs A.11 and A.14 together we have

$$\langle n_z\rangle = \tilde{f}\begin{cases} \left\langle R_0^2(\mu,K)\right\rangle/3N, & \tilde{f}<<1 \\ \left\langle R_0^2(\mu,K)\right\rangle/N - 1/\mu, & \tilde{f}>>1 \end{cases} \tag{A.15}$$

where the Lagrange multiplier μ is the solution of the nonlinear equation

$$1 = \frac{2}{\pi}\int_0^\pi \frac{dq}{G(q)+\mu} + \langle n_z\rangle^2. \tag{A.16}$$

Thus, to obtain all averages, we have to know the integral in the following form

$$\frac{2}{\pi}\int_0^\pi \frac{dq\cos(nq)}{2K+\mu-2K\cos(q)} = \frac{2}{\pi(2K+\mu)}\int_0^\pi \frac{dq\cos(nq)}{1-\beta\cos(q)} = \frac{2}{(2K+\mu)\sqrt{1-\beta^2}}\left(\frac{1-\sqrt{1-\beta^2}}{\beta}\right)^n = \frac{2}{\sqrt{\mu(4K+\mu)}}\left(\frac{1-\sqrt{1-\beta^2}}{\beta}\right)^n \tag{A.17}$$

where $\beta = 2K/(2K+\mu)$ (For evaluation of the integral see G.R. 3.613.128). We can use eq A.17 to obtain the explicit expressions for A.16

$$1-\langle n_z\rangle^2 = \frac{2}{\sqrt{\mu(4K+\mu)}} \tag{A.18}$$

and evaluate the value of

$$\left\langle R_0^2(\mu,K)\right\rangle \approx \frac{2N}{\sqrt{\mu(\mu+4K)}}\frac{1+B}{1-B}, \tag{A.19}$$

where we have introduced

$$B = \beta^{-1} - \sqrt{\beta^{-2}-1} = 1+\frac{\mu}{2K} - \sqrt{\left(1+\frac{\mu}{2K}\right)^2-1} = 1+\frac{\mu}{2K} - \sqrt{\frac{\mu}{2K}\left(2+\frac{\mu}{2K}\right)}. \tag{A.20}$$

Consider two limiting cases

$$B \approx \begin{cases} 1-\sqrt{\mu/K}, & \mu<2K \\ K/\mu, & \mu>2K \end{cases} \tag{A.21}$$

Substitution of these solutions into eq A.19 shows that the value of the Lagrange multiplier, controlling the norm of the unit bond vector, is equal to

$$\mu \approx \frac{\tilde{f}}{\langle n_z \rangle} \tag{A.22}$$

in the large force limit.

This reduces eq. A.18 to

$$1 - \langle n_z \rangle^2 \approx \frac{2\langle n_z \rangle}{\sqrt{\tilde{f}\left(4K\langle n_z \rangle + \tilde{f}\right)}}. \tag{A.23}$$

The force-deformation relation covering the entire interval of the applied force can be described by the following crossover equation

$$\frac{f}{k_B T} \approx \frac{3\langle n_z \rangle}{b_K} + \frac{2\langle n_z \rangle}{b}\left(\sqrt{K^2 + \left(1 - \langle n_z \rangle^2\right)^{-2}} - \sqrt{K^2 + 1}\right). \tag{A.24}$$

To illustrate different regimes of chain deformation, we plot dependence of the reduced force $\tilde{f}/K\langle n_z \rangle$ on the chain deformation parameter $K(1 - \langle n_z \rangle^2)$ in Figure A1. One can clearly identify three different regimes of chain deformation: the freely-jointed chain regime (FJC) in the large force interval, the worm-like chain regime (WLC) in the intermediate force interval, and linear deformation regime where the average value of the projection of the unit vector on the direction of the applied force is proportional to the force magnitude, $\langle n_z \rangle \propto \tilde{f}$. The lines end at points with coordinates (K, $3b/Kb_K$). The crossover to the linear chain deformation regime is manifested by the deviation of the chain deformation curves from the universal line with slope −2, describing chain's deformation in the nonlinear WLC regime.

Appendix B. Simulation Details

We performed simulations of different chain models under tension. First we will outline simulation details for *the discrete chain model with bending potential*. A chain was modeled by a bead-spring chain, consisting of N_m=200 monomers with diameter σ. The monomers were connected into a chain by the finite extension nonlinear elastic (FENE) potential,[29]

$$U_{FENE}(r) = -0.5 k_{spring} R_{\max}^2 \ln\left(1 - \frac{r^2}{R_{\max}^2}\right), \tag{B.1}$$

where k_{spring} is the spring constant, the maximum bond length is $R_{\max}$ = 1.5σ. The repulsive part of the bond potential was modeled by the truncated shifted Lennard-Jones potential. We have performed simulations of chains with $k_{spring} = 100 k_B T/\sigma^2$, $\varepsilon_{LJ} = 1.0\ k_B T$, K=1, 2 and 5 and $k_{spring} = 30 k_B T/\sigma^2$, $\varepsilon_{LJ} = 0.34\ k_B T$ for all other values of the chain bending constants K. The larger value of the spring constant was selected to minimize the effect of the bond stretching at large chain deformations. In our simulations the values of the bond length were equal to b=0.9032 σ and 0.9175 σ for strong and weak spring constants respectively. In the case of the weak bonds the bond length increases to 0.948 (5% increase) for $f\sigma/k_B T$=20, while for the strong bonds it is equal to 0.918 (0.5% increase).

The chain bending rigidity was introduced into the model through a bending potential controlling the mutual orientations between two neighboring along the polymer backbone unit bond vectors $\vec{n}_i$ and $\vec{n}_{i+1}$

$$U_{i,i+1}^{bend}=k_B T\, K(1-(\vec{n}_i\cdot\vec{n}_{i+1})). \tag{B.2}$$

The bending constant K was varied between 1/64 and 160.

The simulations were performed at a constant temperature, which was maintained by coupling the system to the Langevin thermostat. The motion of monomers was described by the following equations,

$$m\frac{d\vec{v}_i(t)}{dt}=\vec{F}_i(t)-\xi\vec{v}_i(t)+\vec{F}_i^R(t), \tag{B.3}$$

where m is the bead mass, $\vec{v}_i(t)$ is the bead velocity, and $\vec{F}_i(t)$ denotes the net deterministic force acting on the i-th bead. The stochastic force $\vec{F}_i^R(t)$ has a zero average value $\left\langle \vec{F}_i^R(t)\right\rangle =0$ and δ-functional correlations $\left\langle \vec{F}_i^R(t)\vec{F}_i^R(t')\right\rangle =6k_B T\xi\delta(t-t')$.[29] The friction coefficient ξ was set to $\xi = 0.143m/\tau_{LJ}$, where τ_{LJ} is the standard LJ-time $\tau_{LJ} = \sigma(m/k_BT)^{1/2}$. The velocity-Verlet algorithm with a time step $\Delta t = 0.01\tau_{LJ}$ was used for integration of the equations of motion eq. B.3. Simulations were performed by using the following procedure: at the beginning of each simulation run, a chain in a random walk configuration was placed in the center of the simulation box. A pair of constant forces f was applied to the both ends of a chain pointing in opposite directions along z-axis. The magnitude of the force was varied between 10^{-3} to 50 k_BT/σ. The system was pre-equilibrated for 2×10^7 MD steps. This was followed by a production run lasting 2×10^8 MD steps. All simulations were performed by using LAMMPS.[29]

Freely-rotating chain model

In addition to simulations of the discrete chain model with bending potential we performed simulations of chains described by the freely-rotating chain model with values of the bond angles θ_0 between 80° and 15°. The values of the bond angles were fixed by imposing a parabolic bond angle potential

$$U_{angle}(\theta)=K_{angle}(\theta-\theta_0)^2 \tag{B.4}$$

where $K_{angle}=300k_BT/rad^2$. The bond length in these simulations was maintained by the FENE and truncated shifted Lennard-Jones potentials with $k_{spring} = 30k_BT/\sigma^2$ and $\varepsilon_{LJ} = 0.34$ k_BT. The Kuhn length for this model is equal to[1]

$$b_K=\frac{b}{\cos(\theta_0/2)}\frac{1+\cos(\theta_0)}{1-\cos(\theta_0)}. \tag{B.5}$$

Chain model with hindered rotations

In order to compare the different models of polymer chains with the models of real chains we performed molecular dynamics simulations of the deformation of chains with dihedral potential corresponding to a coarse-grained model of a polyethylene chain. The bond, bond angle and dihedral angle potentials for this chain model are

$$U=K_{bond}(r-r_0)^2+K_{angle}(\theta-\theta_0)^2+A+B\cos(\phi)+C\cos^3(\phi) \tag{B.6}$$

where r_0=1.526 Å, K_{bond}=260 kcal/mol Å^2, θ_0 = 67.6°, K_{angle}=63 kcal/mol rad^2, A=2 kcal/mol, B = − 4.4 kcal/mol, C=6.4 kcal/mol. The force field parameters for bond and bond angle are from the AMBER force field[30] and the dihedral potential parameters are from Sumpter et al.[16] The simulations were performed at temperature T=300 K. The chain degree of polymerization for these simulations was N_{m}=200. The integration time step was 0.1 ps and simulations continued for 200 ns. The value of the Kuhn length for this model is equal to[1]

$$b_K=\frac{b}{\cos(\theta_0/2)}\frac{1+\cos(\theta_0)}{1-\cos(\theta_0)}\frac{1+\langle\cos(\phi)\rangle}{1-\langle\cos(\phi)\rangle} \tag{B.7}$$

In Table BI we summarized the fitting parameters for force-elongation curves obtained from MD simulations of freely rotating and PE chain models. The quality of the fit is characterized by the value of fit uncertainty σ_{n} (see eq. D.6)

Appendix C. Comparison with Experiments

We applied eq 9 to analyze the force-chain deformation curves for single stranded DNA in salt solutions of different ionic strengths,[17] polymethacrylic acid,[18] polystyrene,[19] polydimethylsiloxane,[20] dextran,[21] methlycellulose,[22] double stranded DNA,[23] N2B domain of titin, and PEVK domain of titin.[24] In experiments one usually measures the average projection of the end-to-end distance $\langle R_z\rangle$ on the direction of the applied force as a function of the force magnitude. Unfortunately, the exact value of the chain degree of polymerization is unknown. Thus, we have modified our eq 8 and considered the size of the fully extended chain R_{max} as an additional adjustable parameter. With this modification, the eq 9 transforms to

$$\frac{f}{k_BT}\approx\frac{3\langle R_z\rangle}{b_KR_{\max}}+\frac{2\langle R_z\rangle}{b_eR_{\max}}\left(\sqrt{K_e^2+\left(1-(\langle R_z\rangle/R_{\max})^2\right)^{-2}}-\sqrt{K_e^2+1}\right) \tag{C.1}$$

where we substituted $\langle n_z\rangle=\langle R_z\rangle/R_{\max}$. The value of the effective bond length b_e for the fitting procedure was set to

$$b_e=b_K\frac{1-\coth(K_e)+K_e^{-1}}{1+\coth(K_e)-K_e^{-1}} \tag{C.2}$$

In Figure C1 we show the results of the least square fitting procedure of the deformation curves of the single stranded DNA molecules of four different lengths stretched at salt concentration 5M [17] to our eq C.1, by considering R_{max}, b_K and K_e as adjustable parameters. The agreement between eq C.1 and the experimental data is very good. The values of the

fitting parameters and of the effective bond length b_e are summarized in Table C1. Note, that the same procedure was used to fit experimental data for all other polymeric systems. For fitting double stranded DNA data we set b_e=0.34 nm which corresponds to the average projection length per base pair.

Using values of the fitting parameters given in Table C1, one can obtain values of the forces that separate different chain deformation regimes shown in Figure 1. In Figure C2 we replotted Figure 1 and added the data points corresponding to the values of the crossover forces obtained from the fitting parameters of the chain deformation curves. The dashed lines in Figure C2 correspond to experimentally accessible force intervals before energetic effects due to bond length and bond angle deformations start to contribute to the chain elasticity.

Appendix D. Comparison of Different Expressions for Chain Deformation

In this section we will establish the accuracy of the different expressions[12, 14] for chain deformations by comparing the expressions with the simulation results for the discrete chain model with bending potential. Below we will compare our expression eq 9

$$\frac{f_{DCR}}{k_BT} \approx \frac{3\langle n_z\rangle}{b_K}+\frac{2\langle n_z\rangle}{b}\left(\sqrt{K^2+\left(1-\langle n_z\rangle^2\right)^2}-\sqrt{K^2+1}\right) \tag{D.1}$$

with expressions derived by Rosa et al[12]

$$\frac{f_R}{k_BT} \approx \left(\frac{3}{b_K}-\frac{1}{b\sqrt{4K^2+1}}\right)\langle n_z\rangle+\frac{1}{b}\left(\sqrt{4K^2+(1-\langle n_z\rangle)^{-2}}-\sqrt{4K^2+1}\right) \tag{D.2}$$

and by Toan and Thirumalai[14]

$$\frac{f_{TT}}{k_BT} \approx \frac{1}{b}\left(\sqrt{4K^2+(1-\langle n_z\rangle)^{-2}}-2K\right) \tag{D.3}$$

which we have rewritten in terms of the parameters of our model and set the exponent α=2 in the Toan and Thirumalai expression.[14] It follows from the eq D.2 that the Toan and Thirumalai expression[14] corresponds to a large force deformation limit of the Rosa et al. expression.[12] In Figure D1 we present the normalized difference between the average value of the projection of the unit bond vector on the force direction obtained from molecular dynamics simulations of the discrete chain model with bending potential, and those obtained from eqs D.1–D.3

$$\Delta n=1-\frac{\left\langle n_z^{th}(\tilde{f})\right\rangle}{\left\langle n_z^{sim}(\tilde{f})\right\rangle} \tag{D.4}$$

It follows from this figure that our expression is the closest to the simulation results with accuracy better than 1% throughout significant interval of the applied forces. Note that in our comparison of the simulation results with the Toan and Thirumalai expression[14] eq. D.3, we only used the interval of the applied forces for which $\langle n_z\rangle > 0.5$. This interval of chain deformations was used by Toan and Thirumalai to fit the experimental data. All expressions

show a very good agreement with the simulation results in the case of strong chain deformations. It should not be surprising since all three expressions converge to the same asymptotic expression in the limit $\langle n_z \rangle \to 1$. However eqs D2 and D.3 show larger deviations from simulation results in the range of intermediate forces.

Let us now solve an inverse problem by considering simulation data as deformation data of a chain with unknown value of the bending rigidity K. By performing this test we will establish how accurate different expressions for chain deformation can recover the value of the chain bending constant. We performed this test for chains with K=1 and K=10. The simulation data were fitted by using the least square fitting procedure by minimizing the difference

$$\chi(K)=\sum_{p=1}^{N_p}\left(1-\tilde{f}^{th}\left(\langle n_z\rangle_p\right)/\tilde{f}_p^{sim}\right)^2 \tag{D.5}$$

with respect to chain bending rigidity K. Summation in eq D.5 is performed over all simulation points N_p. The ratio of b_K/b for this chain model is given by the eq. 3. The accuracy of the fitting procedure was evaluated by calculating the uncertainty

$$\sigma_n=\sqrt{\frac{1}{N_p}\sum_{p=1}^{N_p}\left(\langle n_z\rangle_p^{sim}-\langle n_z\rangle_p^{th}\right)^2} \tag{D.6}$$

The results of this test are listed in Table D1. It follows from this table that our eq. D.1 performs better than eq. D.2 for both sets of simulation data. The largest difference between the actual value of the chain bending constant K and one obtained from the fitting procedure is observed for eq D.2 and data set corresponding to K=1. The fitting method of the simulation data to eq D.2 gives the value of the parameter K equal to K=1.12 with the error of 12% (to be compared with 0.1% error for fitting this data set K=1 by eq D.1). The agreement between actual value of the bending constant and ones obtained from fitting procedure improves with increasing the chain bending rigidity.

Similar tests were conducted for the freely-rotating chain model and the coarse-grained model of a polyethylene chain. Both expressions produced comparable values of the chain bending constants. However, our expression eq D.1 shows smaller value of the uncertainty σ_n (see Table D1).

In the case of the analysis of the experimental data, the number of the fitting parameters increases to three, because in addition to Kuhn length b_K and bending constant K_e, one has to simultaneously optimize the maximum chain length R_{max} (see Appendix C). In this case both fitting by both equations D.1 and D.2 provides close value of the maximum chain length R_{max} (see Table D1). There is a larger difference in the values of the chain bending constant K_e and Kuhn length b_K. The values of uncertainty are close for both fits. This shows that the advantage of a more accurate expression diminishes with increasing the number of the adjustable parameters and the decreasing accuracy of data.

REFERENCES

1. Rubinstein, M.; Colby, RH. Polymer Physics. New York: Oxford University Press; 2003.
2. Treloar, LRG. The Physics of Rubber Elasticity. Oxford: Clarendon Press; 2005.

3. Janmey PA, et al. Negative normal stress in semiflexible biopolymer gels. Nature Materials 2007;6:48–51.
4. Larson RG. The rheology of dilute solutions of flexible polymers: Progress and problems. Journal of Rheology 2005;49:1–70.
5. Minko S. Responsive polymer brushes. Polymer Reviews 2006;46:397–420.
6. Ruhe J, et al. Polyelectrolyte brushes. Advances in Polymer Science 2004;165:79–150.
7. Neuman KC, Lionnet T, Allemand JF. Single-molecule micromanipulation techniques. Annual Review of Materials Research 2007;37:33–67.
8. Neuman KC, Nagy A. Single-molecule force spectroscopy: optical tweezers, magnetic tweezers and atomic force microscopy. Nature Methods 2008;5:491–505. [PubMed: 18511917]
9. Williams MC, Rouzina I. Force spectroscopy of single DNA and RNA molecules. Current Opinion in Structural Biology 2002;12:330–336. [PubMed: 12127451]
10. Marko JF, Siggia ED. Stretching DNA. Macromolecules 1995;28:8759–8770.
11. Bustamante C, Smith SB, Liphardt J, Smith D. Single-molecule studies of DNA mechanics. Current Opinion in Structural Biology 2000;10:279–285. [PubMed: 10851197]
12. Rosa A, Hoang TX, Marenduzzo D, Maritan A. Elasticity of semiflexible polymers with and without self-interactions. Macromolecules 2003;36:10095–10102.
13. Livadaru L, Netz RR, Kreuzer HJ. Stretching response of discrete semiflexible polymers. Macromolecules 2003;36:3732–3744.
14. Toan NM, Thirumalai D. Theory of biopolymer stretching at high force. Macromolecules 2010;43:4394–4400.
15. Carrillo J-MY, Dobrynin AV. Effect of the electrostatic interactions on stretching of semiflexible and biological polyelectrolytes. Macromolecules 2010;43:2589–2604.
16. Sumpter BG, Noid DW, Wunderlich B. Computational experiments on the motion and generation of defects in polymer crystals. Macromolecules 1992;25:7247–7255.
17. Saleh OA, McIntosh DB, Pincus P, Ribeck N. Nonlinear Low-Force Elasticity of Single-Stranded DNA Molecules. Physical Review Letters 2009;102 068301-068301-068304.
18. Ortiz C, Hadziioannou G. Entropic elasticity of single polymer chains of poly(methacrylic acid) measured by atomic force microscopy. Macromolecules 1999;32:780–787.
19. Nakajima K, Watanabe H, Nishi T. Single polymer chain rubber elasticity investigated by atomic force microscopy. Polymer 2006;47:2505–2510.
20. Senden TJ, Meglio J-M, Auroy P. Anomalous adhesion in adsorbed polymer layers. European Physical Journal B 1998;3:211–216.
21. Reif M, Oesterhelt F, Heymann B, Gaub HE. Single molecule force spectroscopy on polysaccharides by atomic force microscopy. Science 1997;275:1295–1297. [PubMed: 9036852]
22. Lee G, Nowak W, Jaroniec J, Zhang Q, Marszalek PE. Molecular dynamics simulations of force conformational transition in 1,6-linked polysaccharides. Biophysical Journal 2004;87:1456–1465. [PubMed: 15345528]
23. Wang MD, Yin H, Landick R, Gelles J, Block SM. Stretching DNA with optical tweezers. Biophysical Journal 1997;72:1335–1346. [PubMed: 9138579]
24. Li H, et al. Reverse engineering of the giant muscle protein titin. Nature 2002;418:998–1002. [PubMed: 12198551]
25. Storm C, Pastore JJ, MacKintosh FC, Lubensky TC, Janmey PA. Nonlinear elasticity in biological gels. Nature 2005;435:191–194. [PubMed: 15889088]
26. Dobrynin AV, Rubinstein M. Theory of polyelectrolytes in solutions and at surfaces. Progress in Polymer Science 2005;30:1049–1118.
27. Sheiko SS, Sumerlin BS, Matyjaszewski K. Cylindrical molecular brushes: Synthesis, characterization, and properties. Progress in Polymer Science 2008;33:759–785.
28. Gradshteyn, IS.; Ryzhik, IM. Table of Integrals, Series and Products. New York: Academic Press; 1965.
29. Plimpton SJ. Fast parallel algorithms for short-range molecular dynamics. J.Comp.Phys 1995;117:1–19. lammps.sandia.gov.

30. Weiner SJ, et al. A new force field for molecular mechanical simulation of nucleic acids and proteins. Journal of the American Chemical Society 1984;106:765–784.

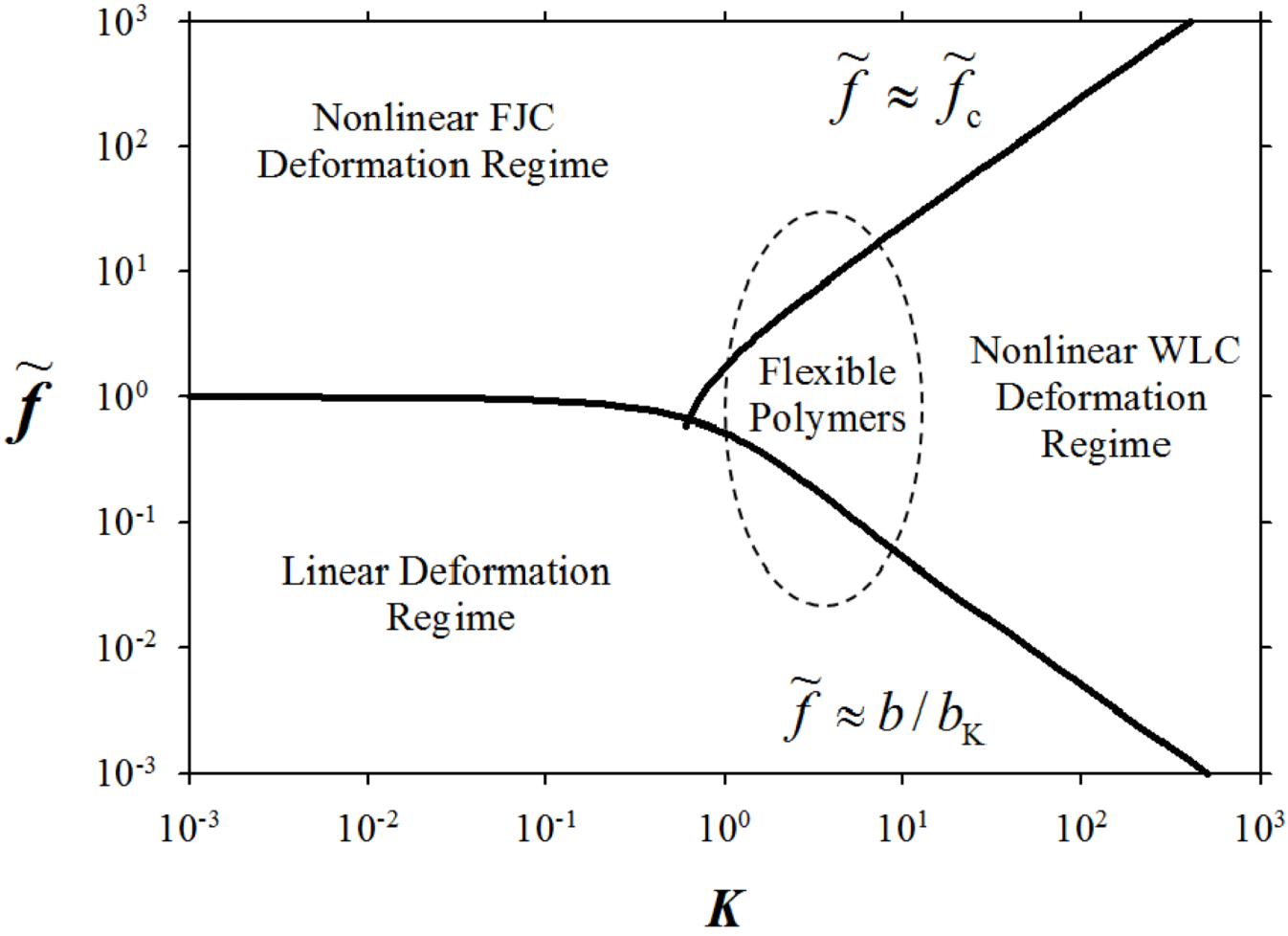

Figure 1.
Diagram of different chain deformation regimes. $\tilde{f} = fb/k_BT$ is a reduced force. Solid lines are given by $\tilde{f} \approx \tilde{f}_c \approx 2.47K(1 - 0.5/K)^{1/2}$ and $\tilde{f} \approx b/b_K = (1 - \coth K + K^{-1})/(1 + \coth K - K^{-1})$ (see text for details). Ellipse shows typical range of parameters corresponding to flexible polymers. Logarithmic scales.

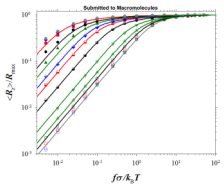

Figure 2.
Deformation of discrete chains with number of monomers N_m=200 and with values of the bending constants: K=1/64 (open hexagons), K =1/32 (open triangles), K =1/16 (inverted open triangles), K =1/8 (open rhombs), K =1/4 (open squares), K =1/2 (open circles), K =1 (crossed triangles), K =2 (inverted crossed triangles), K =5 (half filled circles), K =10 (half filled squares), K =15 (half filled rhombs), K =25 (filled triangles), K =40 (filled circles), K =80 (filled squares), K =120 (filled rhombs), and K =160 (filled hexagons). The lines correspond to eq 9 with no adjustable parameters.

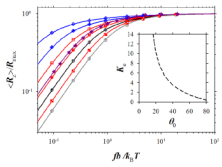

Figure 3.

Deformation curves for freely-rotating chains with the values of the bond angles $\theta_0 = 80°$ (crossed grey hexagons), $\theta_0 = 70°$ (checkered red squares), $\theta_0 = 60°$ (crossed circles), $\theta_0 = 50°$ (red circles with hourglass), $\theta_0 = 40°$ (crossed red squares), $\theta_0 = 30°$ (blue rhombs with hourglass) and $\theta_0 = 20°$ (crossed blue rhombs) and for coarse-grained model of a PE chain (magenta stars). The lines correspond to the eq 9 by using K_e as an adjustable parameter. The values of the fitting parameters are given in Table BI (see Appendix B). The inset shows dependence of the effective bending constant K_e on the value of the bond angle.

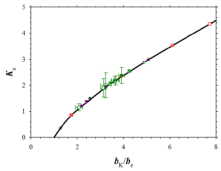

Figure 4.

Dependence of the effective chain bending rigidity K_e on the ratio b_K/b_e of the Kuhn length to the effective bond length for a single stranded DNA at different salt concentrations: 5M (green open squares), 4.0M (green square with a dot), 3.0M (green square, semi-filled right) and 2.0M (green squares, semi-filled left); for PMMA (green squares, semi-filled bottom), polystyrene (green squares, semi-filled top), PDMS (checker green square), dextran (hourglass green square), methylcellulose (magenta open triangle), N2B domain of the protein titin (magenta open inverted triangle), and PEVK domain of the protein titin (magenta filled inverted triangle); and simulation data for freely-rotating chains with the values of the bond angles $\theta_0 = 80°$ (crossed grey hexagons), $\theta_0 = 70°$ (checkered red squares), $\theta_0 = 60°$ (crossed circles), $\theta_0 = 50°$ (red circles with hourglass), $\theta_0 = 40°$ (crossed red squares), $\theta_0 = 30°$ (blue rhombs with hourglass) and $\theta_0 = 20°$ (crossed blue rhombs) and for coarse-grained model of a PE chain (magenta stars). The solid line corresponds to the discrete chain model with bending potential (see eq 11). The data points for this plot are summarized in Tables BI and CI (see Appendices B and C).

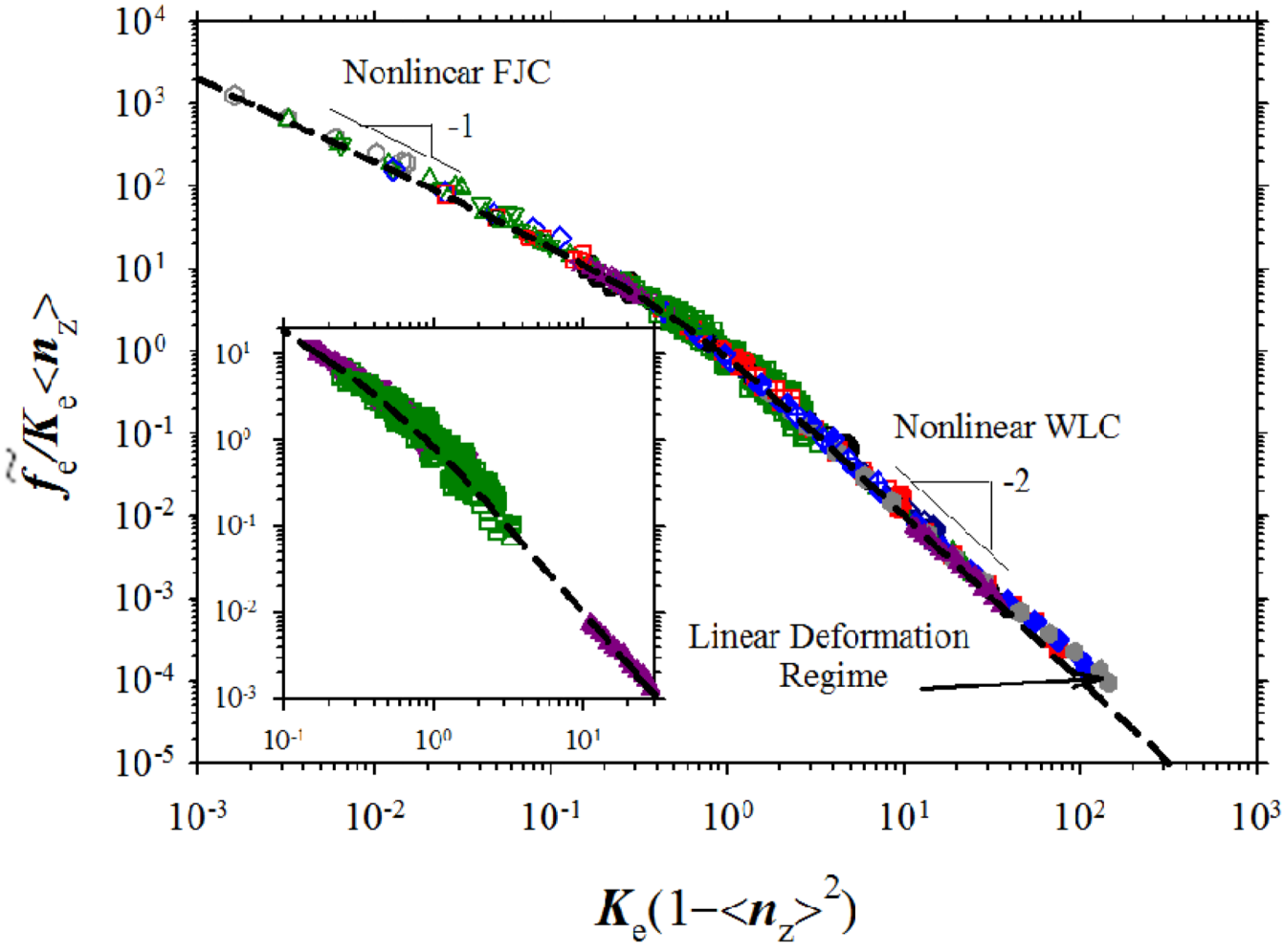

Figure 5.

Universal plot describing deformations of semiflexible chains with bending constants K=1/64 (open grey hexagons), *K*=1/32 (open green triangles), *K*=1/16 (inverted open green triangles), *K*=1/8 (open grey rhombs), *K*=1/4 (open squares), *K*=1/2 (open circles), *K=1* (crossed triangles), *K*=2 (inverted crossed triangles), *K*=25 (half filled circles), *K*=10 (half filled squares), *K*=15 (half filled rhombs), *K*=25 (filled triangles), *K*=40 (filled circles), *K*=80 (filled squares), *K*=120 (filled rhombs), and *K*=160 (filled hexagons); freely-rotating chains with 40° (crossed red squares), 20° (crossed blue rhombs); for coarse-grained model of a PE chain (magenta stars). Experimental data for single stranded DNA at different salt concentrations: 5M (green open squares), 4.0M (green square with a dot), 3.0M (green square, semi-filled right) and 2.0M (green squares, semi-filled left); PMMA (green squares, semi-filled bottom), polystyrene (green squares, semi-filled top), PDMS (checker green square), dextran (hourglass green square), methylcellulose (magenta open triangle), N2B domain of the protein titin (magenta open inverted triangle), PEVK domain of the protein titin (magenta filled inverted triangle) and ddDNA (magenta filled triangle). The value of the reduced force for this plot was calculated as $\tilde{f}_e = fb_e/k_BT$. Inset shows only experimental data.

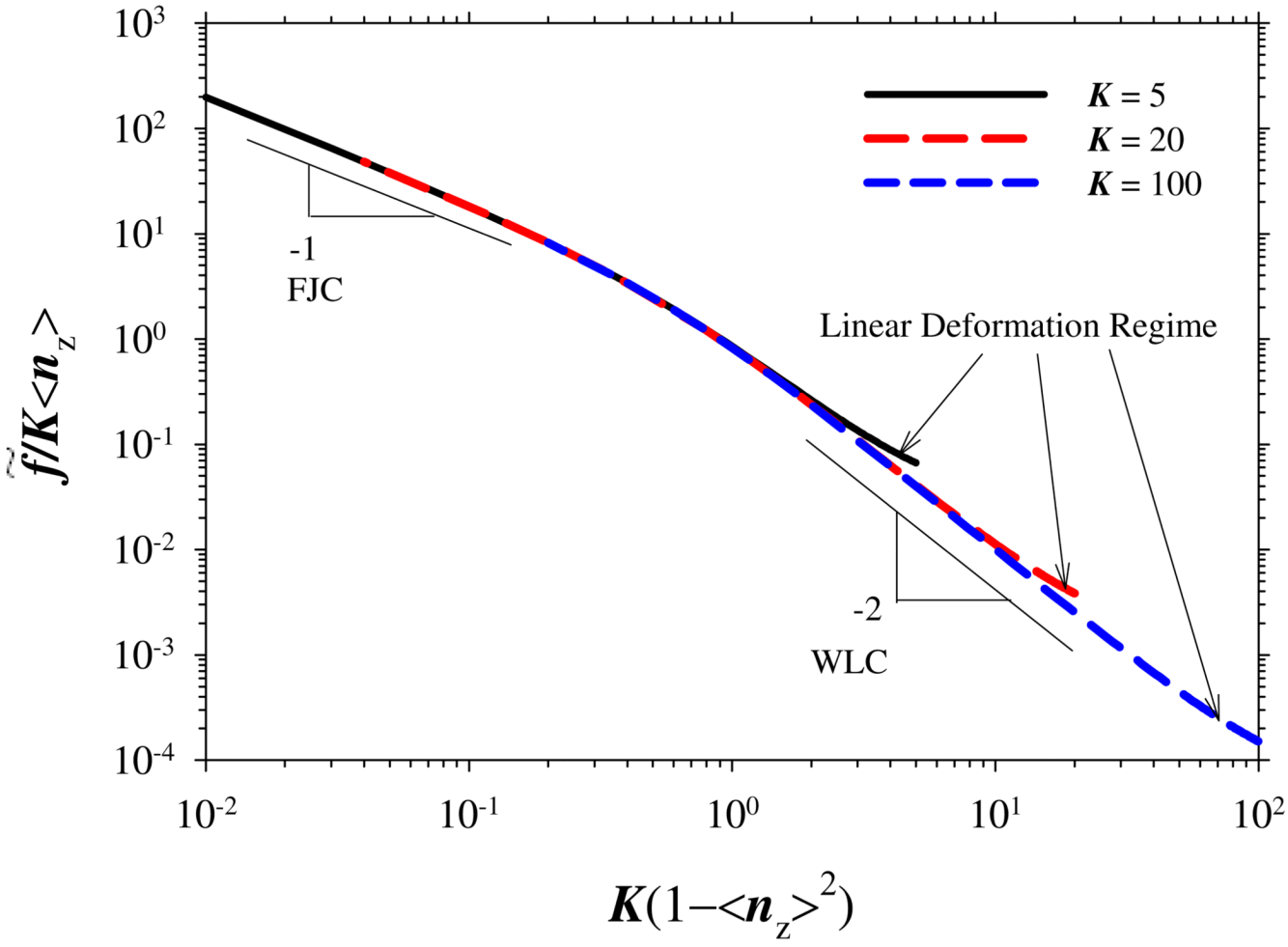

Figure A1.
Universal plot describing deformations of the discrete chain model with bending potential for different values of bending constants.

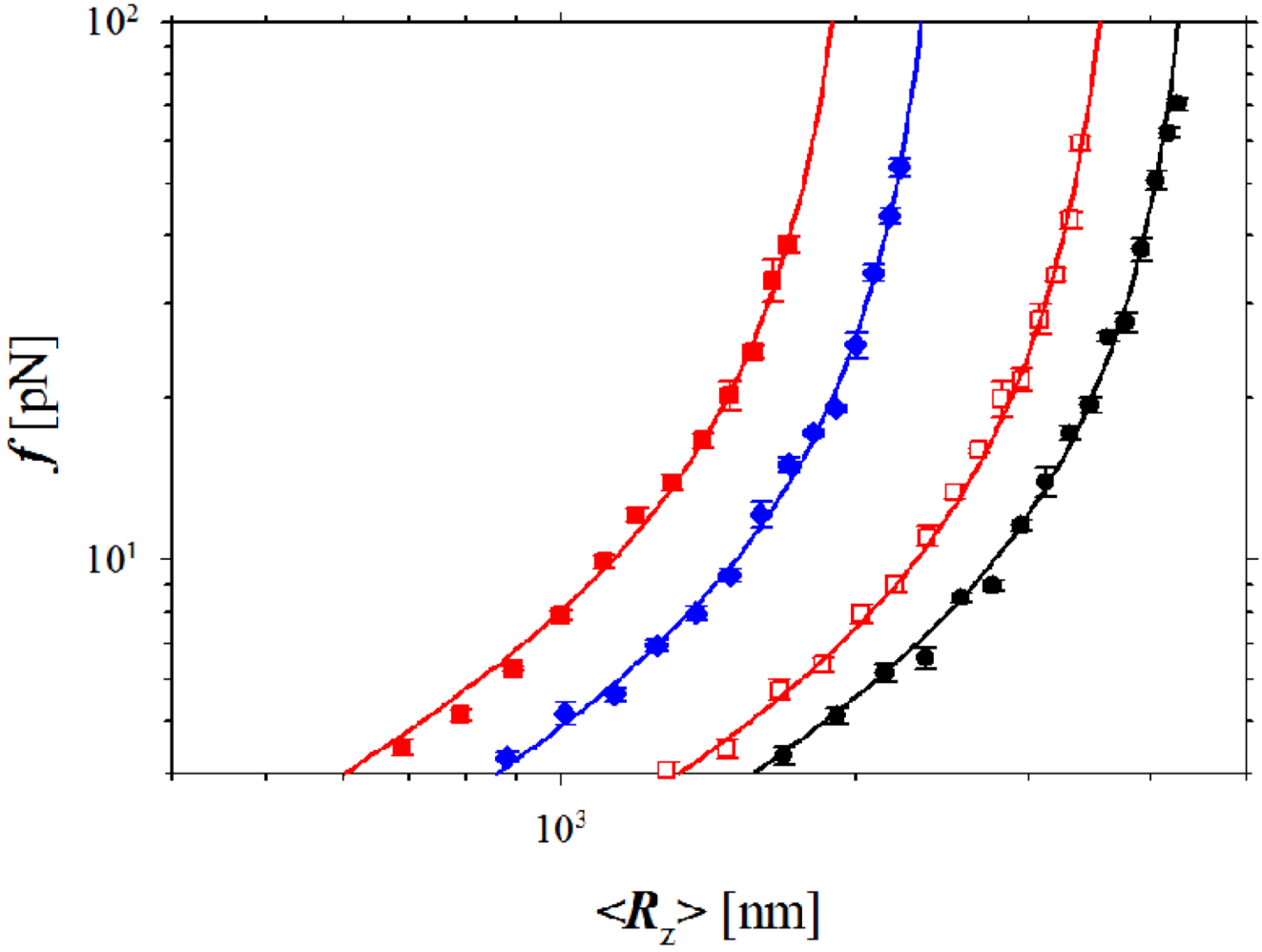

Figure C1.
Dependence of the magnitude of the applied force f on the chain length $\langle R_z \rangle$ for single stranded DNA molecules of four different lengths at salt concentration 5M. The lines are the best fit to the eq. C.1.

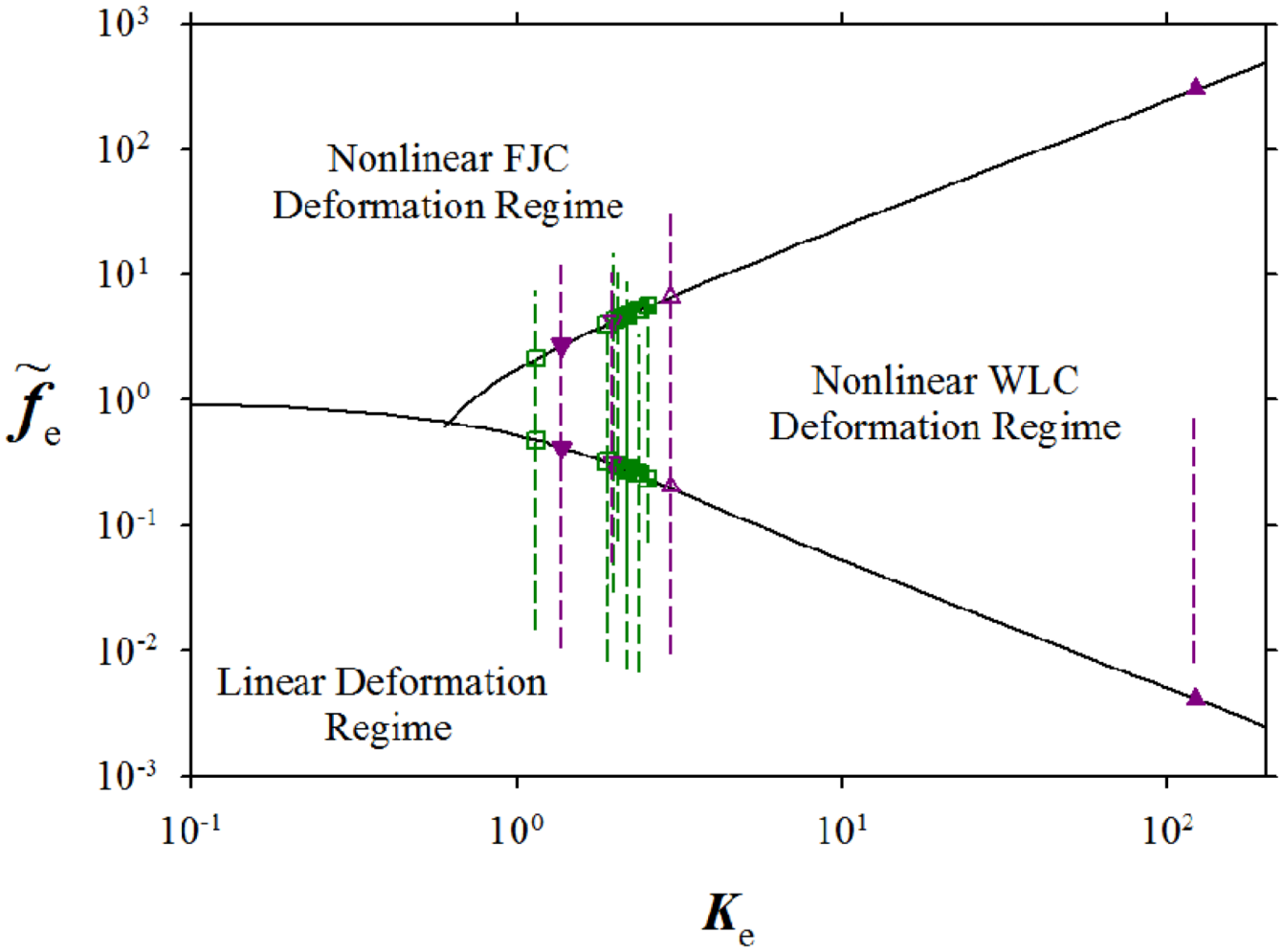

Figure C2.
Diagram of different chain deformation regimes. $\tilde{f}_e = fb_e/k_BT$ is the reduced force. Solid lines represent crossover lines between different chain deformation regimes and are given by the eqs 3 and 8. Dashed lines show the intervals of forces covered in experiments. Logarithmic scales.

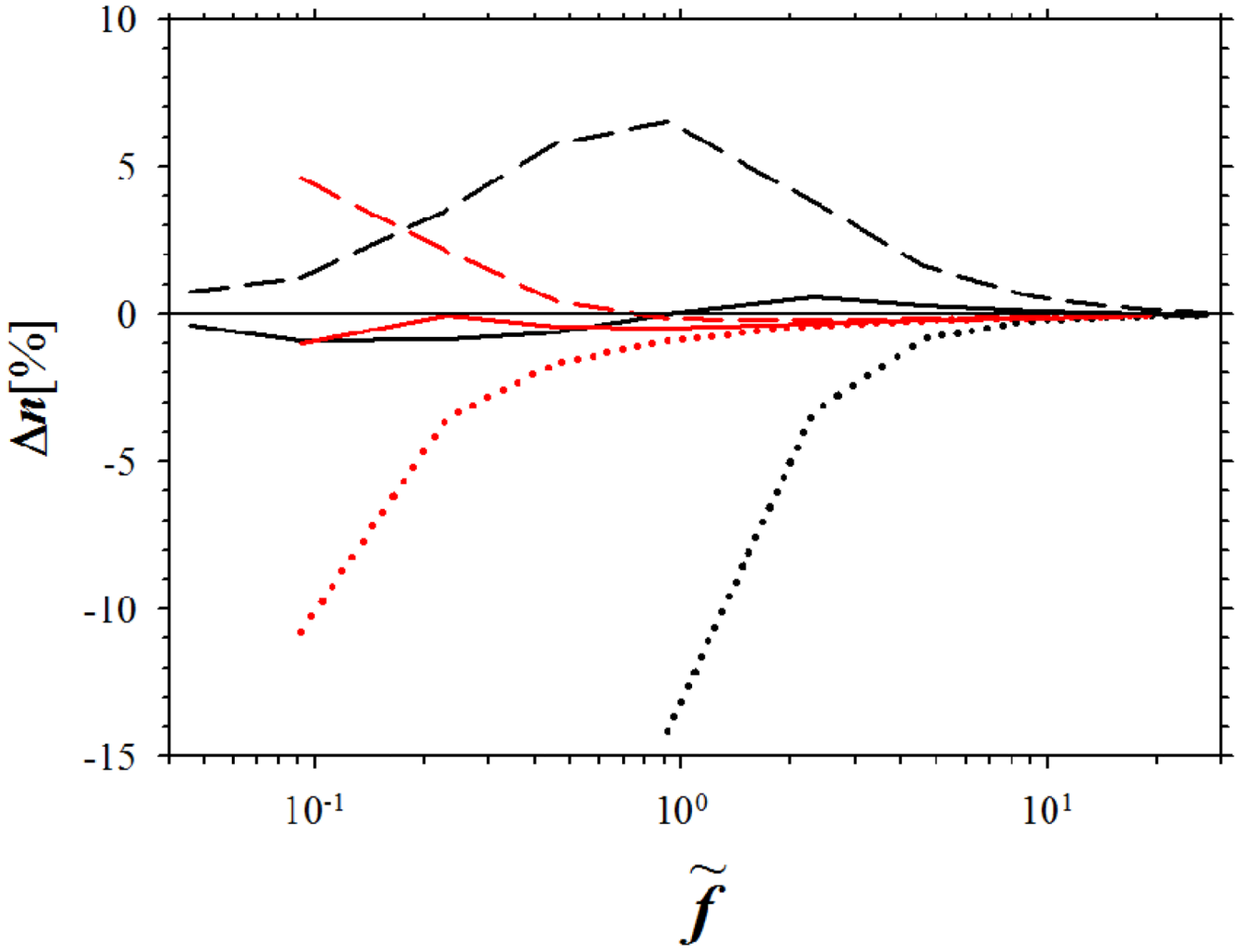

Figure D1.
Dependence of deviation parameter Δn, given by eq D.4, on the reduced force $\tilde{f} = fb/k_BT$. The lines show normalized difference Δn between simulation data and eqs D.1 (solid lines), D.2 (dashed lines), D.3 (dotted lines) for different values of the chain bending constant K=1 (black) and K=10 (red).

Table BI

	b_K	b_e	K_e	σ_n	Legend
Freely rotating chain, $\theta_0 = 80°$	1.701 σ	1.334 σ	0.366	6.3×10^{-3}	grey hexagon, crossed
Freely rotating chain, $\theta_0 = 70°$	2.283 σ	1.309 σ	0.851	6.0×10^{-3}	red square, checker
Freely rotating chain, $\theta_0 = 60°$	3.173 σ	1.245 σ	1.493	4.6×10^{-3}	black circle, crossed
Freely rotating chain, $\theta_0 = 55°$	3.809 σ	1.211 σ	1.890	3.5×10^{-3}	black circle with a dot
Freely rotating chain, $\theta_0 = 50°$	4.641 σ	1.188 σ	2.347	2.5×10^{-3}	red circle, hourglass
Freely rotating chain, $\theta_0 = 45°$	5.764 σ	1.181 σ	2.887	2.2×10^{-3}	inverted green triangle with a dot
Freely rotating chain, $\theta_0 = 40°$	7.329 σ	1.200 σ	3.533	3.0×10^{-3}	red square, crossed
Freely rotating chain, $\theta_0 = 35°$	9.602 σ	1.243 σ	4.357	3.9×10^{-3}	red square with a dot
Freely rotating chain, $\theta_0 = 30°$	13.084 σ	1.313 σ	5.483	4.2×10^{-3}	blue rhombs, hourglass
Freely rotating chain, $\theta_0 = 25°$	18.806 σ	1.406 σ	7.187	3.4×10^{-3}	blue rhombs with a dot
Freely rotating chain, $\theta_0 = 20°$	29.181 σ	1.528 σ	10.051	1.6×10^{-3}	blue rhombs, crossed
Freely rotating chain, $\theta_0 = 15°$	50.880 σ	1.668 σ	15.748	2.3×10^{-3}	blue rhombs, semi-filled right
Hindered rotation model of Polyethylene	0.854 nm	0.393 nm	1.212	1.3×10^{-2}	magenta stars

Macromolecules. Author manuscript; available in PMC 2011 November 9.

Table C1

	b_K (nm)	b_e (nm)	K_e	f_{bK}(pN)	f_c (pN)	Legend
Single-stranded DNA, 5.0 M NaCl buffer [17]	1.15 ± 0.10	0.55 ± 0.07	1.15 ± 0.13	3.58	15.97	green open square
Single-stranded DNA, 4.0 M NaCl buffer[17]	1.11 ± 0.09	0.36 ± 0.04	1.90 ± 0.35	3.71	46.04	green square with a dot
Single-stranded DNA, 3.0 M NaCl buffer[17]	1.27 ± 0.06	0.35 ± 0.02	2.19 ± 0.13	3.24	55.86	green square, semi-filled right
Single-stranded DNA, 2.0 M NaCl buffer[17]	1.33 ± 0.08	0.34 ± 0.04	2.37 ± 0.31	3.09	62.92	green square, semi-filled left
Polymethacrylic acid (PMAA) [18]	0.40 ± 0.04	0.12 ± 0.02	2.00 ± 0.48	10.29	146.68	green square, semi-filled bottom
Polystyrene [19]	0.65	0.19	2.06	6.33	95.88	green square, semi-filled top
Polydimethylsiloxane (PDMS) [20]	0.43	0.10	2.54	9.89	239.09	green square, checker
Dextran [21]	0.72 ± 0.11	0.20 ± 0.02	2.19 ± 0.18	5.71	97.75	green square, hourglass
Methlycellulose [22]	0.48	0.10	2.98	8.51	276.27	magenta open triangle
Double-stranded DNA, 20 mM Tris, 130 mM K^+, 4 mM Mg^{2+} (PTC buffer, pH 8.0) [23]	82.93	0.34	121.96	0.05	3637.84	magenta filled triangle
N2B domain of titin [24]	0.78	0.24	1.97	5.31	72.54	magenta open inverted triangle
PEVK domain of titin [24]	1.40	0.44	1.34	2.95	24.52	magenta filled inverted triangle

Table D1

Inverse problem for discrete chain model with bending rigidity

K_{sim}	K		*Error* (%)		σ_n	
	D.1	**D.2**	**D.1**	**D.2**	**D.1**	**D.2**
1.0	0.999	1.117	0.1	11.7	1.6×10^{-3}	6.1×10^{-3}
10.0	9.750	10.261	2.5	2.6	2.1×10^{-3}	5.7×10^{-3}

Freely-rotating chain model and coarse grained polyethylene chain

	Ke		σ_n	
	D.1	**D.2**	**D.1**	**D.2**
Freely rotating chain, $\theta_0 = 70°$	0.851	0.692	6.0×10^{-3}	1.4×10^{-2}
Freely rotating chain, $\theta_0 = 50°$	2.347	2.147	2.4×10^{-3}	1.4×10^{-2}
Freely rotating chain, $\theta_0 = 20°$	10.051	9.534	1.6×10^{-3}	9.8×10^{-3}
Hindered rotation model of Polyethylene	1.212	0.895	1.3×10^{-2}	1.4×10^{-2}

Single Stranded DNA at 5.0 M NaCl Buffer

	b_K(nm)		b_e(nm)		K_e		R_{max}(nm)		σ_n	
	D.1	**D.2**	**D.1**	**D.2**	**D.1**	**D.2**	**D.1**	**D.2**	**D.1**	**D.2**
1	1.20	1.35	0.66	0.79	0.92	0.82	4518.32	4470.59	1.6×10^{-2}	1.7×10^{-2}
2	0.98	1.1	0.45	0.52	1.22	1.18	2048.79	2032.65	1.3×10^{-2}	1.2×10^{-2}
3	1.22	1.35	0.55	0.73	1.23	0.94	3748.83	3721.01	1.6×10^{-2}	1.7×10^{-2}
4	1.20	1.34	0.55	0.61	1.22	1.25	2492.00	2478.82	1.1×10^{-2}	1.3×10^{-2}
Ave	1.15	1.29	0.55	0.66	1.15	1.05				